J Neurophysiol 100: 1909–1922, 2008.
First published July 23, 2008; doi:10.1152/jn.90684.2008.

Inter- and Intralaminar Subcircuits of Excitatory and Inhibitory Neurons in Layer 6a of the Rat Barrel Cortex

Pratap Kumar[1] and Ora Ohana[1,2]

[1]*Institute of Neuroinformatics, University/ETH Zurich, Zurich, Switzerland; and* [2]*Department of Molecular Neurobiology, Freie Universität Berlin, Berlin, Germany*

Submitted 16 June 2008; accepted in final form 21 July 2008

Kumar P, Ohana O. Inter- and intralaminar subcircuits of excitatory and inhibitory neurons in layer 6a of the rat barrel cortex. *J Neurophysiol* 100: 1909–1922, 2008. First published July 23, 2008; doi:10.1152/jn.90684.2008. Approximately half the excitatory neurons in layer 6 (L6) of the rat barrel cortex project to the thalamus with axon collaterals ramifying in the granular L4; the remaining project within cortex with collaterals restricted to infragranular laminae. In analogy, L6 inhibitory neurons also include locally arborizing and inter-laminar projecting neurons. We examined whether L6 neurons participating in different laminar interactions were also morphologically and electrically distinct. Corticothalamic (CT) neurons were labeled by in vivo injections of a retrogradely transported fluorescent tracer into the primary thalamic nucleus. Whole cell current-clamp recordings were performed from labeled and unlabeled L6 neurons in brain slices of juvenile rats; the morphology of cells was subsequently recovered and reconstructed. Corticocortical (CC) neurons were distinguished from CT cells based on the absence of a subcortical projection and the predominantly infragranular arborization of their axon collaterals. Two morphological CC subtypes could be further distinguished based on the structure of their apical dendrite. Electrically, CT neurons had shorter membrane time-constants and action potential (AP) durations and higher rheobase currents. CC neurons fired high-frequency spike doublets or triplets on sustained depolarization; the burst frequency also distinguished the two morphological CC subtypes. Among inhibitory L6 cells, the L4-projecting ($L6i_{L4}$) and local ($L6i_{L6}$) inhibitory neurons also had contrasting firing properties; $L6i_{L4}$ neurons had broader APs and lower maximal firing rates. We propose that L6 excitatory and inhibitory neurons projecting to L4 constitute specialized subcircuits distinct from the infragranular network in their connectivity and firing patterns.

INTRODUCTION

The appeal of cortical lamina 6 (L6) in the study of sensory information processing arises from its huge potential influence on the responses of both thalamic relay neurons (Gilbert and Kelly 1975; Rouiller and Welker 2000; Wise and Jones 1977) and cortical L4 cells that receive the relay (Ahmed et al. 1994; Fitzpatrick et al. 1985; Gilbert and Wiesel 1979; Zhang and Deschênes 1997). In the rodent somatosensory cortex, this layer is both the widest (Hutsler et al. 2005; Skoglund et al. 1996) and contains the most number of neurons (Ren et al. 1992); it is the infamous heterogeneity in its cell types that makes L6, however, hard to study and its role difficult to understand (Ferrer et al. 1986; Tömböl 1984).

In the rat barrel cortex, the upper portion of this layer (L6a) consists of two main types of excitatory neurons, the corticothalamic (CT) and corticocortical (CC) (Zhang and Deschênes 1997). CT neurons have large terminal arbors in the thalamus and L4, a feature common to other species and cortical areas (Katz 1987; Lund 1988; Prieto and Winer 1999; Usrey and Fitzpatrick 1996); the L4 projection in the primary visual cortex of cats has been estimated to provide about half of all excitatory synapses in that lamina (Ahmed et al. 1994). CC neurons, on the other hand, have extensive intracortical projections but no subcortical target. Inhibitory cells in this lamina can also be divided into two major groups based on their axonal projections, one with inter-laminar axonal projections to granular and supragranular layers and the other with axons restricted to infragranular laminae (Ma et al. 2006; Markram et al. 2004; Tömböl 1984; Wang et al. 2004). Similar interlaminar inhibitory projections have been described arising from infragranular visual cortices of cats and monkeys (Kisvárday et al. 1987; Lund et al. 1988).

L6 could therefore comprise distinct excitatory and inhibitory circuits broadly divisible into those interacting with L4 and those not. It is yet unclear if neurons involved in different subcircuits are also electrically distinct. Recent studies in other cortical regions and laminae have linked specific laminar interconnections with unique biophysical and synaptic properties (Kampa et al. 2006; Morishima and Kawaguchi 2006; Yoshimura et al. 2005); it is proposed that such interactions delineate subcircuits with specialized functions. Cells in L6 with their clearly different inter- and intralaminar projections provide the opportunity to further test this hypothesis.

Attempts to study biophysical differences between excitatory L6 neurons have been few, and the ambiguity in the morphological identity of neurons in these studies leaves the question unanswered (Brumberg et al. 2003; Mercer et al. 2005; van Brederode and Snyder 1992). Biophysical differences between locally arborizing and interlaminar projecting inhibitory neurons in L6 have not yet been investigated. This study asks specifically if the intra- and interlaminar subcircuits in L6 are also associated with unique physiological properties.

METHODS

Experiments were carried out in 37 Wistar rats of both sexes. Briefly, the animals were injected at postnatal day 13–15 with a fluorescent neuronal tracer placed in the ventral posteromedial nucleus (VPm) of the thalamus. Brain slices were obtained from the animals 4–7 days later. Retrogradely labeled corticothalamic neurons and neighboring unlabeled neurons in L6 were targeted for whole cell patch-clamp recordings. All cells were filled with biocytin and their

Address for reprint requests and other correspondence: O. Ohana, Dept. of Molecular Neurobiology, Freie Universität Berlin, Berlin, Takustr. 6 14195 Germany (E-mail: oraohana@neuroscience.fu-berlin.de).

The costs of publication of this article were defrayed in part by the payment of page charges. The article must therefore be hereby marked "*advertisement*" in accordance with 18 U.S.C. Section 1734 solely to indicate this fact.

morphology later recovered and, in some cases, reconstructed. All experiments were carried out under regulations of the Cantonal Veterinary Authority of Zurich.

Thalamic injections

Four or five pups per litter were separated from the dam of which two or three pups were operated on. Animals were anesthetized with a 9:1 mixture of ketamine (63 mg/kg; Narketan, Chassot, Switzerland) and Xylazine (7 mg/kg; Rompun, Bayer Leverkusen, Germany) injected intraperitoneally. The depth of anesthesia was monitored by checking the withdrawal reflex. Animals were placed in a stereotaxic apparatus and their body temperature maintained at 37°C. A fluorescently tagged neuronal tracer, tetramethylrhodamine dextran (TMR-dextran, 3000 MW, Invitrogen Switzerland), was injected into the thalamus at the following coordinates: 3.1 mm posterior and 2.8 mm lateral to Bregma at a depth of 5.3 mm from the dura. Coordinates were modified from Kaneko et al. (1996) to accommodate for the smaller brain size of the young animals used in this study. About 0.2 μl of a 0.1 M solution of TMR-dextran in a citrate buffer (pH 3.0) was slowly pressure-injected using a glass micropipette attached to a pneumatic pump (NeuroPhore BH2, Digitimer). The pipette was left in situ for ~5 min before withdrawing it and repeating the procedure on the other side. Injected animals were allowed to recover from the anesthesia before all the pups, injected or not, were returned to the dam in the home cage.

Slicing procedure

Slices were obtained from injected animals between ages P19 and 22, i.e., 4–7 days after the injection. Animals were rapidly decapitated; the brains were removed and sliced in ice-cold artificial cerebrospinal fluid (ACSF; containing, in mM, 125 NaCl, 2.5 KCl, 25 $NaHCO_3$, 1.25 NaH_2PO_4, 1 $MgCl_2$, 2 $CaCl_2$, and 25 glucose constantly perfused with a mixture of 95% O_2-5% CO_2,). The slicing angle used was a modification of the thalamocortical slice described in mice and rats (Agmon and Connors 1991; Land and Kandler 2002) to have the apical dendrites (and L4-projecting axon collaterals) of L6 neurons oriented parallel to the slice surface. It involved increasing the downward slope of the brain from the 10° used in the studies above to 30°. The blocking cut was retained at 50° to the sagittal plane; this angle also results in slices that are roughly parallel to the barrel rows in L4 (Ajima and Tanaka 2006), such that all the barrels in one slice represent one whisker row on the snout of the animal. About eight 300-μm-thick slices were obtained from each hemisphere and placed in warmed (37°C) ACSF for 30 min. Slices were then allowed to recover at room temperature (21–24°C) for ≥1 h before the recording.

Electrophysiology

All recordings were conducted in a submersion chamber constantly perfused (at 3 ml/min) with oxygenated ACSF maintained at 35°C. Slices and cells were visualized using an upright microscope (Olympus BX61WI) equipped with epifluorescence and infrared differential interference contrast (IR-DIC) optics. TMR labeling in cortex was visualized under epifluorescence at low magnification (10× objective), and its location vis-à-vis L4 barrels was determined under IR-DIC. The orientation of L6 neurons with respect to the slice (and their preservation) was determined by following apical dendrites of fluorescently labeled L6 neurons under high magnification (60× objective) for ~300–400 μm. Recordings were restricted to regions of the barrel cortex with well preserved retrogradely labeled neurons; both labeled and unlabeled L6 neurons in these regions were targeted for whole cell recording.

Somatic whole cell patch-clamp recordings were made in current-clamp mode (Multiclamp-700a amplifier, Molecular Devices); a maximum of two neurons were simultaneously recorded. Patch pipettes (borosilicate, 2 mm OD, 1 mm ID; pipette resistance: 4–8 MΩ) were filled with internal solution containing, in mM, 135 K-gluconate, 4 Mg-ATP, 5 Na_2 phosphocreatine, 0.3 GTP, 10 HEPES, and 4 KCl; osmolarity was adjusted to 280–290 mOsm and pH 7.2. Biocytin (Sigma; 0.25–0.5%) and a green fluorescent dye (Alexa Fluor 488 hydrazide, Invitrogen; 10 μM), were added to the pipette solution prior to recording.

Data acquisition was done on-line through an A-D converter (Digidata 1322, Molecular Devices) at a sampling rate of 10 kHz and filtered at 3 kHz. Liquid-junction potential was corrected, the access resistance continuously monitored, and bridge potential compensated. Typical access resistance under these conditions was between 6 and 25 MΩ. Data were collected and visualized using the pClamp software (Molecular Devices), exported and analyzed off-line, using custom-written routines in Matlab (The Mathworks).

The resting membrane potential (RMP) was measured immediately after establishing the whole cell recording configuration. Various intensities of hyper- and depolarizing rectangular current pulses of 500-ms duration were used to determine basic electrophysiological properties. The time constant of the membrane (τ) was calculated as the time taken to reach 1/e times the minimal membrane potential attained in response to a −50-pA hyperpolarizing current. The input resistance (R_{in}) of the cell was calculated as the slope of the linear fit to the I-V relationship for currents between −70 and 30 pA; steady-state membrane potential values were used.

Properties of the first action potential generated in response to rheobase current (the minimal injected current pulse of 500-ms duration evoking an action potential) were compared between neurons; responses to twice-rheobase current were used to compare properties of spike trains. Spike amplitude was measured from RMP to the peak of the action potential. Spike threshold was calculated as the potential where the second derivative trace of the membrane potential crossed an empirically determined threshold in a small window before the peak; both absolute and relative (to RMP) values are reported. The latency of the spike was defined as the time from the start of the rheobase current pulse to the time at which the threshold for spiking is reached. The threshold-to-peak amplitude was used to measure the spike half-width (HW), which is the full-width at half-amplitude.

Current-frequency (IF) relationships were plotted for both, the average (IF_{avg}) and first instantaneous frequency (IF_1) of the spiking responses to increasing current intensities (500-ms-long pulses). The plots were fit with a function describing an integrate-and-fire neuron (Rauch et al. 2003) as follows

$$F = \frac{F_{max}}{1 + \frac{S}{I - I_0}} \times \theta(I - I_0)$$

The output frequency F is a function of the current, I, and is determined by the following parameters: F_{max}, the saturating value of the firing frequency, S, a steepness factor that is inversely related to the slope of the IF relationship, and I_0, the rheobase current; θ is the Heaviside function that ensures a nonzero output frequency by ignoring currents lower than rheobase. Only cells where sufficient current intensities were injected to cause a saturation of the average firing rate (typically at frequencies ~40 Hz for excitatory neurons) were used in the analysis. Because the currents delivered to each cell differed, the parameters of the fitted model for each cell were used to generate IF curves for currents ranging from 0 to 1 nA. The average and first and second instantaneous frequencies in the spike train (F_{avg}, F_1 and F_2, respectively) and parameters of spike frequency adaptation were calculated for trains evoked by twice-rheobase currents (only for trains with >6 spikes). Each instantaneous frequency was plotted against the time of each successive spike after the first and fit with a single exponential. The adaptation index (AI) is the ratio of the

steady-state frequency to F_1 expressed as a percentage; burst spikes were ignored in measurements of adaptation.

Histological methods

At the end of the recording session, slices were immediately transferred into cold fixative solution containing 4% paraformaldehyde, 0.3% glutaraldehyde, and 15% picric acid in 0.1 M phosphate buffer (PB). Intracellular biocytin was revealed as a black reaction product using the avidin-biotin complex (Vectastain Elite, Rectolab) and a nickel-intensified diaminobenzidine (DAB) reaction. Barrels were revealed using the cytochrome oxidase method (Land and Simons 1985; Wong-Riley and Welt 1980).

Morphological analyses

Axonal and dendritic trees of the biocytin-filled neurons were reconstructed in three-dimension (3D) using the Neurolucida (MicroBrightField) system. Reconstructions were performed using either the ×40 or ×100 oil-immersion objective and not corrected for shrinkage in the z dimension (300 μm thickness of the slice). No obvious shrinkage was observed in the x-y plane, judging from the lack of any tortuosity in the neuronal processes. Dendritic processes were followed to their natural or cut terminations throughout the slice. Axonal processes were however much thinner and often hard to follow through the depth of the slice; the reconstructions are therefore incomplete; only axons with total reconstructed length >1500 μm were included in the analysis. Thickness of CT and CC descending axons were measured 150 μm below the soma; however, the accuracy of measurements of fine caliber axons is limited by the diffraction limit of light microscopy (~0.25 μm). Terminations resulting from the slicing process (top and bottom artificial ends) are treated differently from those due to inadequate filling and difficulties in visualization, which occur within the slice thickness (middle artificial ends). All reconstructions were imported into the Matlab environment, where they were analyzed and plotted using custom-written routines. The cells are presented such that the left (negative x) side is the postero-medial direction in cortex and toward the larger barrels in the row; the positive x-direction points anterolaterally and toward the smaller barrels.

Cortical dimensions were measured in every slice in which a neuron was reconstructed. Three laminar boundaries could be discerned in all these slices, the pial surface, lower border of L4 and the white matter (WM), and distances of the soma from these boundaries were measured. The average L4-WM thickness (infragranular thickness; 1,088 ± 97 μm; n = 57 slices) was used to normalize the vertical dimensions of neurons. The normalization factor (NF) was calculated for each neuron as the ratio of the L4-WM distance in its slice to the average infragranular thickness and only the vertical dimensions were multiplied by the NF. Measures of axonal and dendritic dimensions with respect to laminar boundaries were made on the normalized data while tree structure analyses were performed on the unaltered reconstructions.

Statistical analyses were performed using t-test; the Kolmogorov-Smirnov test was used in cases where the data were not normally distributed. The Bonferroni correction was used when multiple pairwise comparisons were made between two populations. Alpha values used were 0.0042 and 0.0031 for morpho- and physiological data, respectively (alpha of 0.05 divided by 12 and 16 independent comparisons). Receiver-operator curves (ROC) were calculated for parameters that differed significantly between two populations.

RESULTS

Retrograde labeling of CT cells

An essential element of this study is the unambiguous identification of CT neurons in L6. This was achieved by injecting a dye into the VPm thalamic nucleus where the CT neurons in L6 form terminal axonal arborizations; retrograde transport of the dye therefore selectively labels this subset of L6 neurons. Brain slices visualized 4–7 days after the injections of TMR-dextran into the VPm thalamic nucleus showed a single, wide band of labeled cell bodies in L6 of the barrel cortex (Fig. 1*A*). The retrograde somatic labeling was restricted to the upper half of L6, while a diffuse neuropil stain was seen in L4, most likely reflecting the anterograde labeling of thalamocortical axon terminals (though axons of L6 cells may also contribute to this label; Fig. 1*B*). Discrete, large fluorescent points seen in L4 and L5 are nonspecific signals arising from blood vessels or debris and none is neuronal. This pattern of labeling suggests that the injections were restricted to the VPm and did not involve the posterior (Po) nucleus of the thalamus (Herkenham 1980; Koralek et al. 1988). Both labeled (TMR-positive/CT) and unlabeled (TMR-negative) somata in L6 were targeted for whole cell recordings (Fig. 1*C*).

Excitatory neurons in L6

Data from a total of 72 excitatory and 34 inhibitory neurons are presented, all of which were morphologically identified; data from the two classes of neurons are presented separately. Of the excitatory cells, 34 were identified as CT by being TMR-positive; the rest were TMR-negative and selected based on morphological criteria described in the following text.

It has been estimated that about half of all pyramidal neurons in L6 in the rat barrel cortex project to the thalamus (CT), with the other half projecting to the second somatosensory, motor or peri-rhinal cortices but not subcortically, and therefore termed corticocortical, or CC (Zhang and Deschênes 1997). All TMR-positive (CT) neurons in our data had a thick axon (0.61 ± 0.1 μm; n = 10; measured 150 μm below the soma) that entered (or headed toward) the white matter before being severed by the slicing process. The population of CC neurons was defined as TMR-negative pyramidal cells without a prominent principal descending axon as illustrated in Fig. 2*A*. The descending axons of these neurons were of thinner gauge (0.3 ± 0.06 μm; n = 10), showed multiple en passant boutons, and rarely entered the white matter. In cases where a branch did extend into the white matter, it could be followed for long distances along the subcortical plate, a course very different from that of CT cells, which descend into the striatum en route to the thalamus. The two main pyramidal populations in L6, CT and CC, could therefore be distinguished based on the retrograde label and the structure of the descending axon; reconstructions of seven examples of each shown in Fig. 2*B* illustrate this point.

CT neurons were spiny pyramidal neurons of moderate size with somatic diameters of 10–15 μm and an area of 137 ± 43 μm^2 (n = 21). The average distance from the pial surface to the soma was 1,430 ± 129 μm (n = 34). The entire layer 6 extends from ~1,300 to 1,900 μm below the pial surface; the CT neurons recorded and reconstructed in this study were therefore restricted to the upper portion of L6 (L6a). Spiny (presumed excitatory) TMR-negative cells that were classified as CC were also mostly pyramidal neurons (28 of 38) but also included cells of inverted pyramidal, bipolar, or a nonspecific morphology; this study is restricted to data obtained from pyramidal CC neurons. The size and depth of the somata of CC pyramidal cells (151 ± 43 μm^2 and 1,452 ± 176 μm, respec-

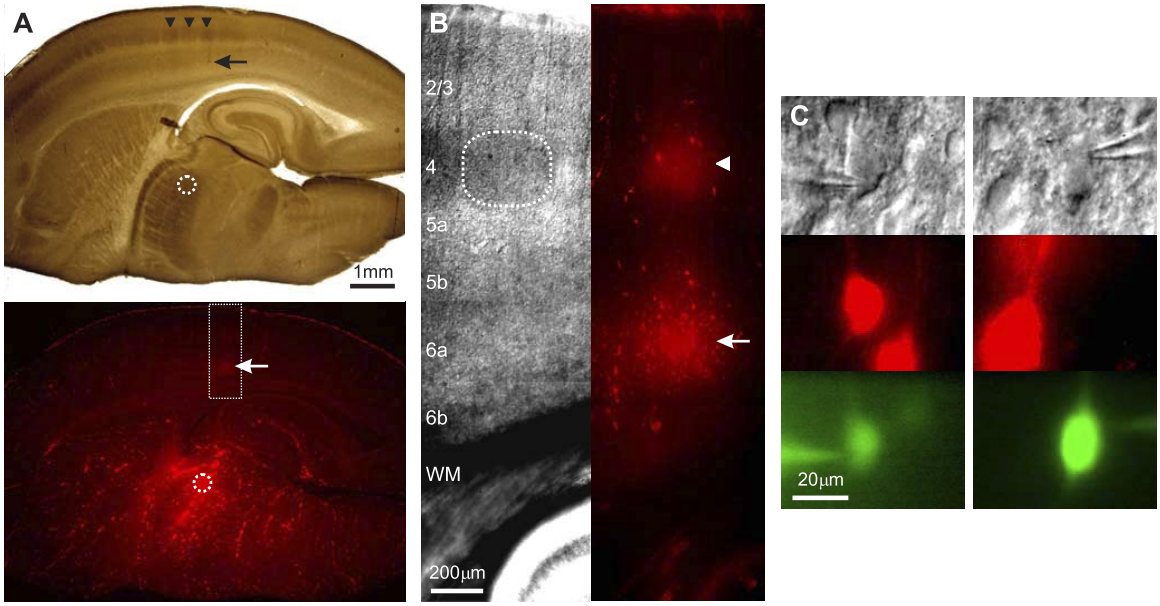

FIG. 1. Retrograde labeling of corticothalamic (CT) neurons. *A, top*: brain slice processed for cytochrome oxidase, revealing barrels in L4 (arrowheads), and also for intracellular biocytin, revealing recorded neurons in layer 6 (L6; arrow). The circle indicates the region of the ventral posteromedial nucleus (VPm) targeted by the injection. *Bottom*: fluorescent signal from the same slice; a bright signal is seen originating from the injection site (white circle corresponds to the target region above) and a weaker signal in cortical L6 (arrow). The cortical region bounded by the box is magnified in *B*. *B*: magnified image (10×) of the region of the slice bounded in *A* seen under differential interference contrast (*left*) and fluorescence (*right*). Cortical layers are labeled and a L4 barrel outlined. Two distinct regions of fluorescent labeling are seen, 1 in L4 (arrowhead) and the other in L6 (arrow), the former arising from the neuropil and the latter including cell somata. *C*: higher magnification (60×) of 2 L6 neurons that were targeted for whole cell recording. *Left*: the cell was labeled by the injection of tetramethylrhodamine (TMR)-dextran in the VPm (seen in the red channel; *middle panels*). Both cells were loaded with Alexa 488 (green fluorescence; *bottom*) and biocytin via the recording pipette.

tively; $n = 23$ and 28) did not differ from that of CT neurons. L6 CT neurons cannot therefore be distinguished based on the IR-DIC image of the acute slice, i.e., by somatic shape, size, or location.

Apart from the qualitative axonal differences between CT and CC neurons described in the preceding text, further differences could be quantified. Descending axons of CT neurons gave fewer branches than those of CC neurons (3.9 ± 1.3 vs. 7.8 ± 2.4, $P = 1.1e^{-6}$; $n = 16$ and 19, respectively); first branches originated from the principal axon at similar distances from the soma for both cell types (72 ± 14 vs. 81 ± 19 μm), but while all CT axon branches arose within ~200 μm from the soma, CC axons continued to branch deeper in L6a and even in L6b (distances from soma to last branch: 152 ± 62 vs. 292 ± 133, $P = 6.6e^{-4}$); these differences are plotted in Fig. 2*C*. The orientation of axon collaterals also differed. Collaterals of CT neurons arose normal to the principal axon but quickly turned upwards to head toward L4 in a columnar fashion. CC axon collaterals, on the other hand, extended horizontally in the infragranular laminae for long distances. This vertical bias of CT axons and the relatively uniform radial distribution of CC axons with respect to the soma (Fig. 2*D*) are apparent in the maximal axonal span (222 ± 89 vs. 661 ± 205 μm, $P = 1.0e^{-7}$) and percentage of axonal length within L6 (58 ± 14 vs. 93 ± 12%, $P = 5.2e^{-6}$) for the two groups.

Dendrites of CT and CC neurons

Dendrites of CT cells, like their axons, were stereotypic. About six basal dendrites radiated out from the soma, each branching once to twice on average, and together spanning a region 220 μm in diameter around the soma. A thicker apical dendrite arises from the top of the soma and rises toward the pial surface to end either within L4 or just below. The apical dendrite initially gives off a skirt of oblique branches and then continues to ascend relatively unbranched through L5 finally ending in a tuft of branches in the region around L4; each section constitutes about a third of the total length of the apical dendrite. Dendritic trees of all reconstructed CT cells are displayed in Fig. 3*A* in ascending order of dendrite length in L4. Cells with apical tufts ending below L4 are therefore on the left, and those with a tuft completely in L4 on the right. The level at which the tuft ends appears correlated to the depth of the soma in L6. The data therefore represent a continuum of neurons distributed within the upper part of L6, with no clear groups emerging from within the CT population based on either the apical tuft or other dendritic parameters as seen by Zhang and Deschênes (1997). Inadequate preservation of axons in the slice precludes such an analysis from being performed on the axon collateral innervation of L4 and L5a.

The CC population, unlike the CT, does seem to comprise of more than one cell type. From the pyramidal neurons classified as CC based on axonal morphology, it is possible to discern at least two subtypes based on dendritic morphology. This is illustrated in Fig. 3*B*, where the dendritic structure of a variety of CC neurons is represented. The first six reconstructions are examples of one type of CC neuron. This type of cell has been described previously in vivo by Zhang and Deschênes (1997), these were short pyramidal cells with a "star-like" appearance due to a decreasing length and number of apical oblique branches with increas-

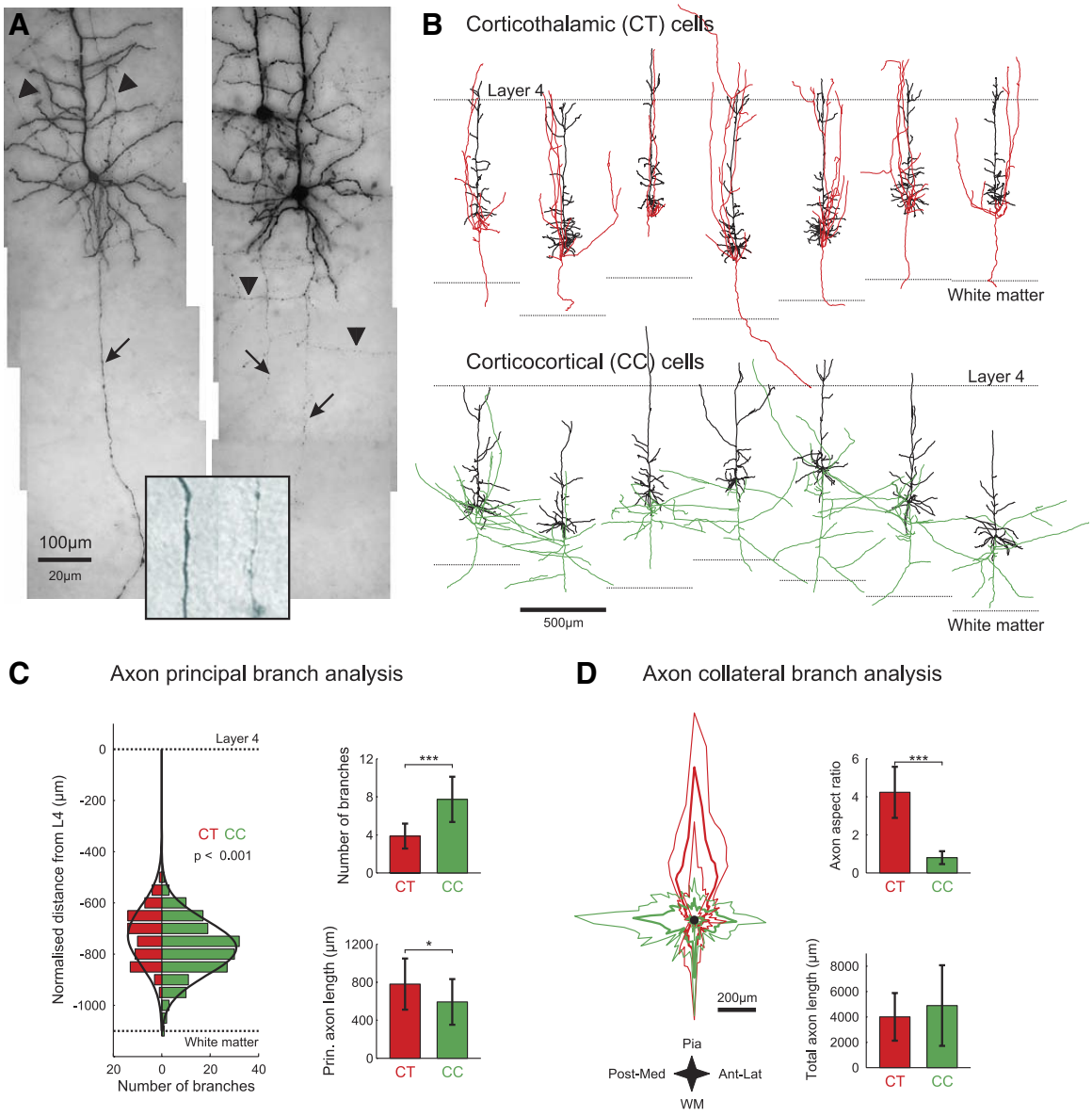

FIG. 2. Distinguishing CT and corticocortical (CC) neurons in L6. *A*: photomontages of a TMR-positive (*left*) and 2 TMR-negative (*right*) neurons in L6 stained with biocytin; the somata, proximal dendrites, and descending axons of each cell are seen. The principal descending axon (arrow) of the TMR-positive (and therefore CT) neuron is thick, gives out a few branches close to the soma that turn upward (arrowheads), and then descends toward the white matter. Descending axons of TMR-negative cells are thin (arrow), with branches arising at various distances from the soma and extending horizontally in L6 (arrowheads). Inset: a higher-magnification view of adjacent CT (*left*) and CC axons in the same slice taken 150 μm from the soma. *B, top*: reconstructions of 7 CT neurons (soma and dendrites in black, axons in red). *Bottom*: reconstructions of 7 TMR-negative neurons (axons in green), which show a contrasting axonal branching pattern. Corticocortical (CC) neurons are defined based on the lack of retrograde label and the presence of a relatively thin and branched descending axon and horizontally oriented axonal collaterals. The lower boundary of L4 has been aligned in each reconstruction. *C*: histogram of the number of primary branches arising at various depths of cortex. The distance between L4 and the white matter in each reconstruction was normalized to an average infragranular thickness (see METHODS); this allows a comparison of the morphology of different neurons with respect to cortical lamination. Primary branches of CT axons arise higher in L6; the bold lines are single Gaussian fits to each distribution. CT axons have fewer primary branches along with a greater length of the principal descending axon preserved in the slice; data from 16 CT and 19 CC neurons. *D*: quantification of axonal orientation with respect to the slice. *Left*: total length of axonal segments oriented in each of 90 angular bins around the soma (black dot); data represent 16 CT and 16 CC neurons with >1,500 μm of reconstructed axon (thick and thin lines represent means and SDs, respectively). The aspect ratio of this plot (maximal vertical vs. maximal horizontal extent) shows the vertical bias of CT axons; the total reconstructed axon in each group does not vary (*right*). *, $P < 0.05$; **, $P < 0.01$; ***, $P < 0.001$.

ing distance from the soma; we labeled this group CC1. Another type of TMR-negative pyramidal neuron is illustrated in the next group of nine reconstructions. The apical dendrites of these cells, while also ending without an obvious tuft, display long oblique branches all along their ascent through L5. These branches give the neurons a candelabrum-like appearance; we termed this group CC2.

CC1 and CC2 cells made up most of the corticocortical cells encountered. Other pyramidal CC types included cells with a long, slender apical dendrite ending in L3 or higher, resembling claustrum-projecting cells described in the cat visual cortex by Katz (1987) and neurons with a prominent apical tuft like those of CT cells. Examples of these latter types of pyramidal neurons as well as those of nonpyramidal cells of

bipolar and inverted pyramidal morphology are also illustrated in Fig. 3*B*. The analyses in this study are focused on the three main pyramidal cell types encountered, i.e., CT, CC1, and CC2.

The somata and dendritic trees of all reconstructed cells of the CT, CC1, and CC2 groups are overlaid in Fig. 3*C;* the vertical dimension of the trees have been normalized as described in METHODS. This view illustrates the coverage of

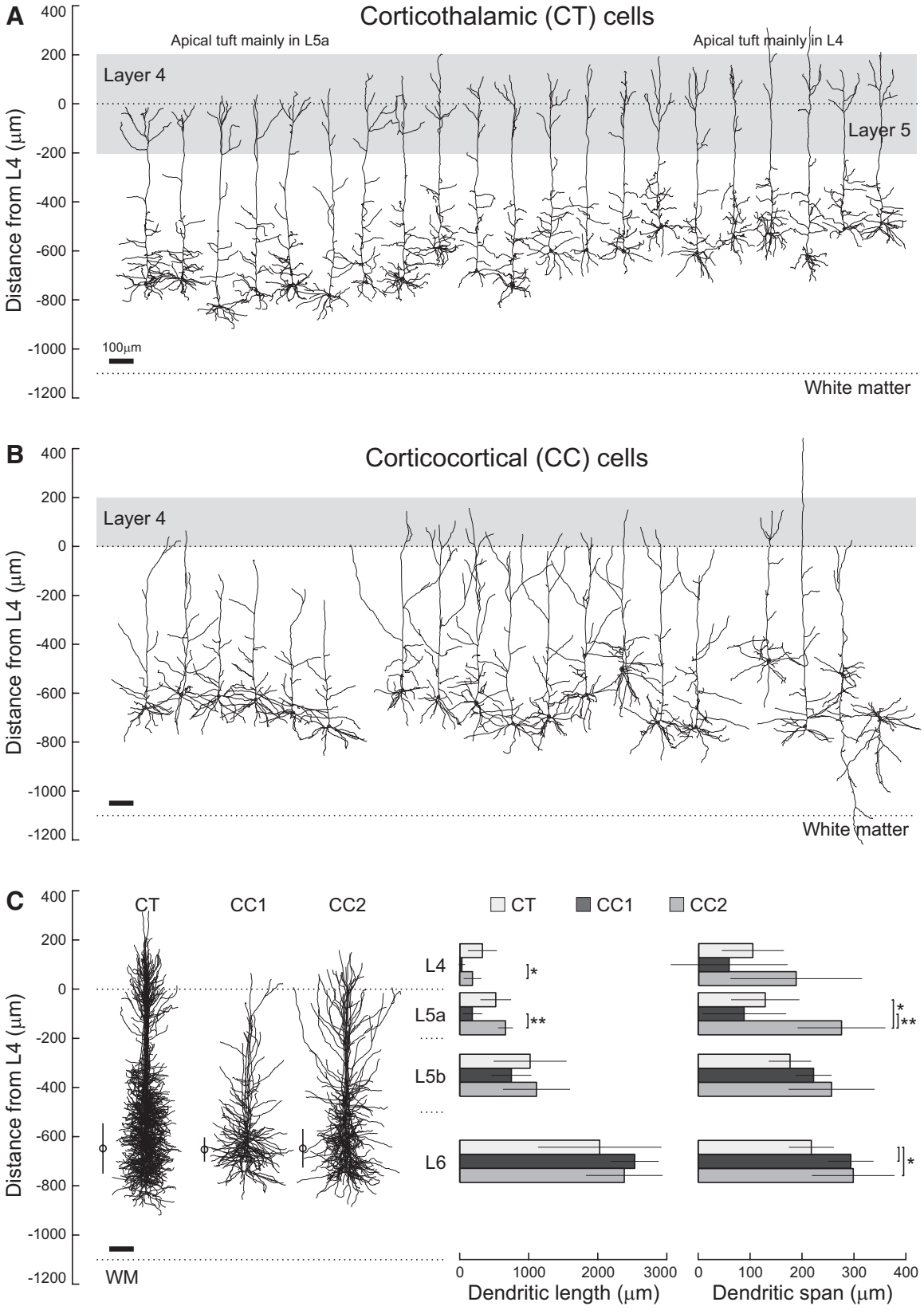

cortical space by the dendrites of the different cell types. Coverage is quantified in two aspects: the total dendritic length and the maximal horizontal span, both as a function of cortical lamination; these are plotted on the right for each of the three groups. CT cells have a narrower dendritic span compared with CC cells in general (233 ± 59 vs. 337 ± 59 μm; $n = 21$ each). Other differences are specific to the subgroups of CC cells; for example, CC1 cells have lesser dendritic length and narrower dendritic spans in L4 and L5a compared with both CC2 and CT cells. Somata of both CT and CC cells in this sample are located at similar depths within L6 (1,430 ± 129 vs. 1452 ± 176 μm below the pia, and 632 ± 119 vs. 652 ± 108 μm below L4); they also did not differ in size. However, the total surface area (soma + dendrites) of CT cells tends to be less than that of CC neurons (7,934 ± 1,802 vs. 10,137 ± 3,185 μm^2, $P = 0.011$); the significance of this difference did not however overcome the stringent Bonferroni correction for multiple pair-wise comparisons. All morphological parameters of CT, CC1 and CC2 neurons are summarized in Table 1.

In summary, the dendritic integration and axonal projection spaces of CT and CC neurons in L6 vary. CT neurons appear to both receive from and send information to L4, while CC neurons project their axons and dendrites mainly within the infragranular laminae. A new finding is the existence of two distinct pyramidal CC subtypes based on their dendritic structure; further study would be required to reveal any corresponding difference in axonal structure.

Physiological properties of CT, CC1, and CC2 neurons

The morphology of a neuron determines to an extent its biophysical and firing properties (Bekkers and Häusser 2007; Mainen and Sejnowski 1996). The physiological properties of the three morphological subtypes of L6 pyramidal neurons were therefore examined. Data were obtained from 34 CT and 28 CC neurons; of the latter, 6 were classified as CC1 and 11 as CC2. The rest either could not be classified due to inadequately recovered dendritic morphology ($n = 6$) or belonged to distinctly different pyramidal subtypes ($n = 5$).

The resting membrane potential (RMP) of CT and CC neurons was close to −70 mV, and the input resistance was also similar (146 ± 47 and 152 ± 56 MΩ, $P = 0.6$). The membrane time-constant (τ_{memb}), however, varied significantly between CT and CC cells (12 ± 2.7 vs. 16.6 ± 3.7 ms, $P = 6.5e^{-7}$). Further differences were seen in the spiking properties of the three cell types, both in the nature of the individual action potential as well as spike trains. First the current intensities required to bring CT neurons to their spiking thresholds were significantly higher than those required for CC cells (196 ± 80 vs. 129 ± 46 pA, $P = 6.3e^{-4}$). This measure, the rheobase of the neuron, is used as the reference stimulus intensity for the comparison of single spike properties of different neurons. The first spikes discharged in response to rheobase current differed between the CT and CC neurons in their latency from the start of the pulse (67.9 ± 22.1 vs. 140.3 ± 44.9 ms, $P = 7.9e^{-10}$) and half-width (0.77 ± 0.13 vs. 1.01 ± 0.2 ms, $P = 1.2e^{-9}$); the difference in spike width is due to a steeper falling phase of the action potentials in the former (54 ± 16 vs. 82 ± 14 mV/ms). The fall slope of the spike also differentiates CC1 and CC2 neurons, but while a difference in half-width is also seen, it does not overcome the Bonferroni correction. These properties of exemplar CT and CC cells as well as population averages are illustrated in Fig. 4*A*.

Trains of action potentials elicited in response to increasing current intensities revealed further differences among CT, CC1, and CC2 cell types. All three responded with regular spike trains in response to 500-ms-long depolarizing current pulses, but the CC neurons fired high-frequency doublets and triplets in the beginning of the spike trains even at low current injections; responses to twice-rheobase currents in three exemplar neurons are illustrated in Fig. 4*B*. A minority of the CT neurons (2 of 34), but none of the CC cells showed phasic (2–3 action potentials followed by no spiking) spike responses. These spiking differences are highlighted in the current-frequency (*I-F*) relationships plotted in Fig. 4*C*. No differences between the three groups were seen when the average train frequency (F_{avg}) was plotted against the injected current. However, the first instantaneous frequency (F_1) relationship to current was clearly different in the examples shown and in the population averages. CC1 neurons fired the most obvious burst spikes in response to the smallest currents, resulting in the steepest I-F_1 curve; CC2 responses were mainly in the form of doublets of slightly lower frequencies compared with CC1 cells, while CT neurons never fired in burst mode. The first- and second-instantaneous frequencies in response to twice-rheobase currents and the I-F_1 curve slopes clearly distinguished each pyramidal cell type in L6 (Fig. 4*D*). The physiological features of different excitatory L6 neurons are summarized in Table 2.

Because it is unlikely for the thalamic injections to have labeled the complete CT population in the barrel cortex, TMR-negative cells could be either CC or unlabeled CT neurons. A group of TMR-negative neurons, ($n = 22$) had a morphology indistinguishable from TMR-positive (CT) neurons: all displayed thick descending axons with rising collaterals and an apical dendritic tuft in L4. This group of neurons also resembled CT neurons in all of their physiological parameters. The remaining TMR-negative pyramidal neurons constituted the CC group which displayed homogenous morphological and physiological properties distinct from those of the CT neurons.

Inhibitory L6 neurons

Data from 32 inhibitory L6 neurons (L6i) were recorded, some of which had an obvious nonpyramidal morphology in

FIG. 3. Dendritic features of CT and CC neurons. *A*: dendrites and somata of 21 CT neurons arranged with respect to the length of apical tuft in L4 vs. L5a (shaded regions); the vertical dimension of all reconstructions have been normalized with respect to the L4-white matter (WM) distance as described in METHODS. No clear distinction can be seen with respect to the L4 or L5 location of the apical tuft of CT neurons. *B*: CC neurons with qualitatively different dendritic trees. Apical dendrites of the 1st 6 (from left) cells resemble fir trees with progressively shorter and fewer apical oblique branches (CC1). The next 9 have long oblique branches in L5, giving them a candelabrum-like appearance (CC2). CC neurons with other dendritic morphologies were also encountered, but less frequently; examples of these include, from right, inverted pyramidal and bipolar neurons, pyramidal cells with a thin apical dendrite extending into L3 and others with an obvious apical tuft. *C*: quantification of dendritic innervation of the slice by CT, CC1, and CC2 neurons. *Left*: the soma and dendrites of 21 CT, 6 CC1, and 9 CC2 neurons are overlaid, centered on their somata. The mean depth of the somata in L6, and SD, are shown alongside each group. The total dendritic length and maximal dendritic span of each cell type are compared with respect to cortical lamination on the *right*. *, $P < 0.05$; **, $P < 0.01$.

TABLE 1. *Morphological parameters of CT, CC1, and CC2 pyramidal neurons*

Morphological Parameters	CT (21)	CC (22)	*P* Value	ROC Area	CC1 (6)	CC2 (11)	*P* Value	ROC Area
Dist. from pial surface, μm	1430 ± 129	1452 ± 176	0.58		1600 ± 177	1397 ± 144	1.2E-02	0.81
Dist. from L4-L5 border, μm	−632 ± 119	−652 ± 108	0.57		−729 ± 107	−622 ± 96	3.7E-02	0.79
Depth from slice surface, μm	−27.4 ± 12.3	−25.1 ± 10.3	0.53		−19.0 ± 4.9	−27.5 ± 10.9	0.11	
Soma horizontal diameter, μm	11.8 ± 2.1	12.6 ± 2.0	0.15		12.3 ± 2.2	12.8 ± 2.1	0.79	
Soma area, μm^2	136.7 ± 43.2	151.1 ± 42.7	0.53		153.3 ± 36.2	150.2 ± 46.2	0.89	
Soma + dend. area, μm^2	7934 ± 1802	10137 ± 3185	8.7E-03	0.75	11962 ± 3463	9408 ± 2865	0.10	
Basal dendrite length, μm	1266 ± 412	1478 ± 432	2.9E-02	0.67	1649 ± 240	1409 ± 477	0.40	
Apical dendrite length, μm	2602 ± 510	2438 ± 477	0.53		2031 ± 456	2601 ± 390	9.3E-03	0.87
No. of total ends	25.7 ± 5.2	20.8 ± 4.6	**1.1E-03**	**0.85**	21.3 ± 4.9	20.6 ± 4.6	0.53	
No. of cut ends	9.9 ± 3.2	9.0 ± 4.1	0.45		6.7 ± 2.7	10.0 ± 4.2	0.09	
No. of basal dendrite branches	22.5 ± 7.4	24.2 ± 5.0	0.37		24.3 ± 2.2	24.1 ± 5.9	0.99	
No. of apical dendrite branches	44.1 ± 8.5	30.1 ± 7.2	**1.3E-06**	**0.92**	26.0 ± 5.6	32.9 ± 5.7	2.1E-02	0.80
Avg. basal branch order	2.1 ± 0.3	2.4 ± 0.3	9.3E-03	0.72	2.3 ± 0.2	2.4 ± 0.3	0.39	
Avg. apical branch order	9.8 ± 1.6	7.1 ± 1.3	**2.2E-07**	**0.93**	6.2 ± 0.8	7.6 ± 1.0	4.7E-03	0.85
Percentage of dendrite in L4	8.7 ± 5.7	4.2 ± 3.9	4.3E-03	0.75	0.8 ± 1.3	5.5 ± 3.8	1.4E-02	0.88
Percentage of dendrite in L5a	13.4 ± 5.0	10.7 ± 5.4	0.10		4.9 ± 3.7	13.0 ± 4.1	**4.9E-04**	**0.92**
Percentage of dendrite in L5b	27.0 ± 14.4	27.6 ± 16.0	0.97		21.6 ± 6.2	30.1 ± 18.2	0.29	
Percentage of dendrite in L6	50.6 ± 16.6	57.1 ± 20.3	0.26		72.7 ± 9.8	50.8 ± 20.2	2.2E-02	0.87
Percentage of dendrite in L4 + L5a	22.1 ± 5.1	14.7 ± 7.0	**1.5E-03**	0.77	6.8 ± 4.4	18.5 ± 4.9	**2.1E-04**	**0.96**
Max. dendritic span, μm	232 ± 39	341 ± 58	**9.8E-09**	**0.95**	318 ± 45	350 ± 61	0.26	
Dend. span in L4, μm	114 ± 53	169 ± 115	0.07		191 ± 161	165 ± 115	0.79	
Dend. span in L5a, μm	131 ± 65	191 ± 107	0.03		119 ± 78	215 ± 106	0.08	
Dend. span in L5b, μm	174 ± 42	256 ± 78	**1.3E-04**	**0.82**	238 ± 35	263 ± 88	0.51	
Dend. span in L6, μm	218 ± 44	300 ± 84	**3.2E-04**	**0.85**	314 ± 48	294 ± 96	0.64	
Total axon length, μm	3970 ± 1811	5041 ± 3315	0.27					
Descending axon length, μm	781 ± 269	595 ± 247	0.03	0.76				
No. of axonal branches	24.0 ± 11.3	33.6 ± 19.0	0.29					
No. of primary branches	3.9 ± 1.3	7.8 ± 2.4	**1.1E-06**	**0.94**				
Soma to first branch, μm	71.9 ± 14.1	80.6 ± 19.0	0.08					
Soma to last branch, μm	151.5 ± 61.5	291.7 ± 133.1	**6.6E-04**	**0.86**				
Max. axonal span, μm	222 ± 89	661 ± 205	**1.0E-07**	**0.98**				

Somatic, dendritic, and axonal parameters of the three pyramidal cell types in L6. Tree lengths with respect to laminar boundaries are calculated after the normalization explained in the methods; absolute lengths reported are of the unaltered reconstructions. Parameters differing significantly after the Bonferroni correction ($P < 0.0042$) are indicated in bold. Number of neurons are in parentheses. CT, Corticothalamic; CC1 & CC2, corticocortical 1 and 2, respectively; ROC, receiver-operate curve.

the DIC image. The identity of each cell was confirmed by light microscopy based on morphological criteria such as smooth or beady dendrites and dense axonal ramifications with large boutons (Martin et al. 1983; Ribak 1978). In occasional cases when no structure was recovered, the neuron was considered to be inhibitory if it either displayed high-frequency spike trains with minimal accommodation ($n = 4$) as defined in Gupta et al. (2000) or if an inhibitory effect could be directly measured in another neuron ($n = 1$).

Based on the axonal morphology of L6i cells that were recovered ($n = 27$), two distinct anatomical types of L6i cells could be identified. The first class of inhibitory neurons, described classically as basket cells, had axons ramifying within infra-granular layers, with no restriction by columnar or laminar boundaries visible in their arborization. Both large and small basket-like cells were encountered, differing mainly in the density and extent of their axonal arbors. Because most of the axon of these neurons was restricted to the infragranular laminae, we labeled them L6-targeting L6i neurons or $L6i_{L6}$. In contrast, another set of inhibitory L6 cells encountered showed distinct laminar preferences in their axonal arborization. The axon of these cells arose from the top of the soma to give three to four branches within L6 (or deep in L5) that descended back into L6, densely innervating the region around the soma. The main trunk (or 2–3 branches) continued to ascend to branch again within or just below L4 with the most profuse collateral branching innervating upper L4 and lower L3. This creates a clear bilaminar innervation zone in layers 6 and 4, earning these neurons the label of L4-targeting L6i cells, or $L6i_{L4}$. Of the 32 inhibitory cells in our data, 9 could be classified as $L6i_{L4}$ and another 9 as $L6i_{L6}$; the rest could not be reliably classified into either of the two classes, either due to insufficient filling of the axon or because the axon was severed too early (e.g., in lower L5) to make the distinction.

Physiologically the two types of L6i neurons differed in the properties of both single spike and spike trains. Single spikes elicited by rheobase currents in $L6i_{L6}$ cells were narrower than those in $L6i_{L4}$ neurons (0.37 ± 0.06 vs. 0.63 ± 0.07 ms, $P = 6.2e^{-6}$). The rheobase current itself was higher in $L6i_{L6}$ neurons (220 ± 37 vs. 129 ± 57 pA, $P = 7.3e^{-3}$) and the amplitude of the spike also smaller (74.1 ± 5.5 vs. 82.6 ± 6.8 mV, $P = 0.02$) than in the $L6i_{L4}$ cells; the differences in rheobase and spike amplitude did not however overcome the Bonferroni correction for statistical significance.

On sustained depolarization, $L6i_{L6}$ neurons tended to fire high-frequency trains with minimal adaptation. Both average and first instantaneous frequencies in response to twice-rheobase current were higher in these neurons compared with $L6i_{L4}$ neurons (165 ± 50 vs. 64 ± 33 Hz, $P = 7.4e^{-4}$ and 201 ± 48 vs. 88 ± 23 Hz, respectively, $P = 1.1e^{-4}$) as well as the maximal saturating frequencies (221 ± 37 vs. 129 ± 57 Hz, $P = 3.0e^{-3}$). Spike

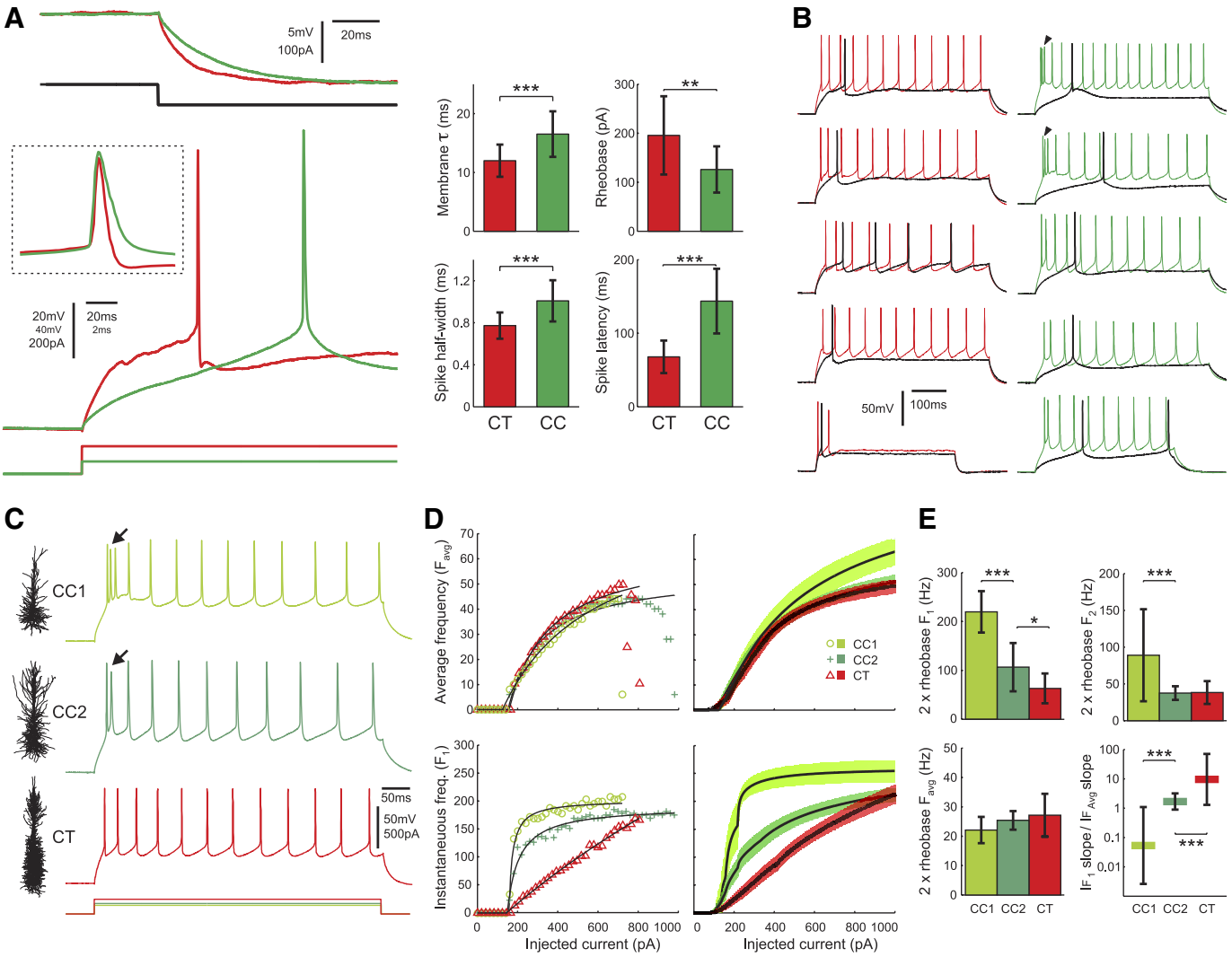

FIG. 4. Physiological differences between CT and CC neurons. *A*: examples of single CT and CC neurons illustrating differences in the membrane time constant measured in response to a −50-pA pulse (*top*). The rheobase currents (*bottom*) and action potential latencies (*middle*) and widths (*inset*) for spikes evoked by the rheobase current also vary. All these parameters are compared for 34 CT and 38 CC neurons on the *right*. *B*: responses to rheobase (black traces) and twice-rheobase currents in 5 CT (*left,* red traces) and CC (*right,* green traces) neurons. CC neurons respond with doublets or triplets (arrowheads) to moderate depolarizing currents. Phasic responses were rarely observed but only in CT neurons (*bottom left trace*). *C*: spike trains elicited in exemplar CC1, CC2, and CT neurons by twice-rheobase currents (*bottom*). CC1 neurons show greater burst-like responses than CC2 neurons (arrows). *D*: current-frequency (IF) relationships for exemplar cells (*left*) from each group for both average spike frequency (IF_{avg}; *top*) and 1st instantaneous frequency (IF_1; *bottom*). Black lines are the fits with an integrate-and-fire neuron model described in METHODS. The fits for all neurons in each group are averaged on the *right;* black lines are means, shaded regions SDs (n = 6, 11 and 34 for CC1, CC2, and CT groups, respectively). *E*: comparisons of spiking parameters measured in response to twice-rheobase currents for each group. The 1st (F_1) and 2nd (F_2) instantaneous spike frequencies vary between cell types, but the average spike frequency responses (F_{avg}) to the 500-ms pulse are similar. The ratios of the slopes of the IF_1 and IF_{avg} plots also differentiate the 3 cell types.

frequency adaptation in both cell types were comparable at twice-rheobase currents though $L6i_{L4}$ neurons did show greater adaptation in trains evoked by lower currents.

The two inhibitory groups therefore, like the morphologically distinct excitatory cells, are also associated with contrasting physiological properties. This is graphically illustrated in Fig. 5, where along with the morphology of two exemplar neurons of each class, four physiological parameters are plotted. Two of these, the rheobase current and spike half-widths, when plotted against each other, result in separate clusters for each morphological type: $L6i_{L6}$ cells are associated with a higher rheobase and narrower spikes compared with $L6i_{L4}$ neurons. A few exceptions to this pattern are observed suggesting that locally arborizing neurons could include subtypes with differing physiology, as seen in the basket cell population in general (Wang et al. 2002). The physiological parameters of inhibitory neurons and the differences between the two L6i cell types and those between inhibitory and excitatory neurons in general, are summarized in Table 3.

DISCUSSION

Anatomical data show that L6 neurons participate in both a thalamocortical circuit involving L4 and a highly integrative infragranular intracortical network (Zhang and Deschênes 1997). In this study, we have undertaken to characterize the morphology and electrical properties of L6 neurons that participate in either of these networks. We show that L6 neurons

TABLE 2. *Physiological parameters of CT, CC1, and CC2 pyramidal neurons*

Physiological Parameters	CT (34)	CC (38)	*P* Value	ROC Area	CC1 (6)	CC2 (11)	*P* Value	ROC Area
RMP, mV	−70.2 +/− 3.6	−70.5 +/− 4.5	0.76		−71.0 +/− 3.4	−70.6 +/− 4.9	0.86	
Input resistance, MΩ	146.2 +/− 47.0	152.1 +/− 56.2	0.63		133.3 +/− 32.4	154.0 +/− 38.9	0.26	
Membrane tau, ms	**12.0 +/− 2.7**	**16.5 +/− 4.0**	**6.5E-07**	**0.84**	18.1 +/− 3.4	16.4 +/− 3.7	0.33	
Rheobase, pA	**195.6 +/− 79.8**	**133.4 +/− 56.5**	**6.3E-04**	**0.77**				
AP1 amplitude, mV	101.7 +/− 6.7	102.0 +/− 8.8	0.89					
AP1 latency, ms	**67.9 +/− 22.1**	**137.1 +/− 50.6**	**7.9E-10**	**0.92**				
AP1 half-width, ms	**0.77 +/− 0.12**	**1.02 +/− 0.16**	**1.2E-09**	**0.88**	0.85 +/− 0.15	1.08 +/− 0.17	7.4E-0.3	0.84
AP1 rise slope, mV/ms	99.3 +/− 18.5	105.1 +/− 22.6	0.24		106.3 +/− 27.0	107.8 +/− 17.4	0.88	
AP1 fall slope, mV/ms	**−79.1 +/− 13.8**	**−50.7 +/− 13.2**	**3.6E-13**	**0.93**	**−68.3 +/− 9.4**	**−45.1 +/− 9.9**	**7.7E05**	**0.94**
AP1 threshold-absolute, mV	−30.4 +/− 5.0	−32.2 +/− 4.7	2.4E-02	0.62				
AP1 threshold-relative, mV	40.0 +/− 4.4	38.3 +/− 4.5	0.10					
AP1 fAHP amplitude, mV	**−13.7 +/− 3.4**	**−9.4 +/− 4.2**	**1.1E-05**	**0.78**				
AP1 sAHP amplitude, mV	−17.1 +/− 2.9	−15.5 +/− 4.5	0.74					
AP1 fAHP latency, ms	**4.4 +/− 3.4**	**9.0 +/− 5.3**	**4.8E-07**	**0.82**				
AP1 sAHP latency, ms	**17.6 +/− 7.6**	**63.7 +/− 26.3**	**7.3E-15**	**0.93**				
Max avg frequency, Hz	39.0 +/− 14.8	48.9 +/− 12.8	0.08		51.6 +/− 17.7	46.2 +/− 10.0	0.42	
Max 1st inst. frequency, Hz	**142.1 +/− 57.4**	**223.8 +/− 59.6**	**1.5E-06**	**0.83**	268.7 +/− 47.1	198.2 +/− 64.6	4.2E-02	0.82
Max 2nd inst. frequency, Hz	74.1 +/− 35.9	121.0 +/− 59.2	3.9E-03	0.75	169.5 +/− 63.2	95.8 +/− 48.0	1.6E-02	0.83
2×Rheobase: Avg. freq., Hz	28.4 +/− 6.1	25.0 +/− 6.4	3.1E-02	0.70	24.3 +/− 4.0	24.7 +/− 4.8	0.86	
2×Rheobase: 1st inst. freq., Hz	**61.7 +/− 24.3**	**140.1 +/− 69.6**	**2.3E-05**	**0.87**	**224.5 +/− 39.9**	**108.8 +/− 50.1**	**3.2E-04**	**0.97**
2×Rheobase: 2nd inst. freq., Hz	36.4 +/− 12.2	53.7 +/− 37.2	4.3E-02	0.63	**101.3 +/− 50.7**	**37.2 +/− 11.6**	**3.8E-04**	**0.91**
2×Rheobase: adaptation index	**54.1 +/− 11.2**	**80.0 +/− 10.4**	**1.2E-12**	**0.95**	91.0 +/− 1.1	75.6 +/− 11.2	8.4E-03	1.00
2×Rheobase: adaptation tau, ms	**20.9 +/− 14.2**	**6.9 +/− 5.0**	**2.3E-05**	**0.86**	4.6 +/− 1.7	8.6 +/− 7.1	0.23	
IFavg fit: saturation freq, Hz	59.0 +/− 20.0	78.8 +/− 37.6	4.6E-02	0.70				
IFavg fit: 1/slope	175.5 +/− 92.5	348.2 +/− 295.5	0.05					
IFavg fit: rheobase, pA	196.3 +/− 76.2	162.6 +/− 71.9	4.6E-02	0.64				
IFinst fit: saturation freq, Hz	758.1 +/− 967.6	306.5 +/− 201.6	1.4E-02	0.63				
IFinst fit: 1/slope	**1817.0 +/− 2341.1**	**332.3 +/− 643.0**	**5.8E-04**	**0.77**				
IFinst fit: rheobase, pA	215.3 +/− 133.2	172.9 +/− 82.0	0.26					
IFinst fit slope/IFavg fit slope	**10.78 +/− 8.50**	**1.27 +/− 1.83**	**2.9E-07**	**0.95**	**0.05 +/− 0.05**	**1.44 +/− 1.72**	**3.5E-04**	**1.00**

A comparison of physiological properties of CT and CC neurons (*left*) and CC1 and CC2 neurons (*right*). *P* values of *t*-tests and ROC areas for each differing parameter ($P < 0.05$) are listed. Parameters differing significantly after the Bonferroni correction ($P < 0.0031$) for are indicated in bold. Number of neurons are in parentheses. RMP, resting membrane potential; AHP, after hyperpolarization.

projecting to L4 have electrical properties that clearly distinguish them from those ramifying in infragranular laminae. We propose that L4-projecting excitatory and inhibitory L6 neurons compose, together with their L4 targets, discrete cortical subcircuits that are tuned for specific manipulations of the sensory information.

Morphology of excitatory L6 neurons

The labeling pattern in the barrel cortex following injections in the VPm was similar to earlier studies (Herkenham 1980; Killackey and Sherman 2003) and the morphology of CT (TMR-positive) neurons recorded in vitro closely resemble those previously described in vivo (Zhang and Deschênes 1997). We used the consistent and stereotypic morphology of this class of neuron as a template to compare unlabeled pyramidal cells with contrasting axonal (CC) morphology. Unlabeled neurons that morphologically resembled CT cells also resembled them physiologically, thus supporting the criteria used for identifying CC neurons in this study.

CT cells in our sample likely include neurons projecting to the VPm alone and those targeting both VPm and Po thalamic nuclei; the two were previously reported to have different sites of apical tuft and axon collateral ramification (Killackey and Sherman 2003; Zhang and Deschênes 1997). However, dendritic tufts of CT cells reconstructed in this study form a continuum between being located completely within L4 to completely below L4 (Fig. 3*A*). Neither dendritic tufts nor physiological properties (tested between cells at extreme ends of the distribution) could distinguish two CT types. Anatomical differences between CT neurons may therefore also reflect a difference in somatic depth (with apical dendrite length remaining constant), and ergo, neural birth time.

The two CC neuron types distinguished here have counterparts reported in earlier studies, CC1 cells described as starlike by Zhang and Deschênes (1997) and CC2 as nontufted pyramidal neurons by Zarrinpar and Callaway (2006); we report differences in dendritic length and span as a function of cortical lamination between the two. CT neurons have narrower dendritic spans than either of the CC subtypes and greater dendritic lengths in L4, suggesting that inputs to each population arise from different regions of the cortical column (Zarrinpar and Callaway 2006). CT cells may receive far greater L4 and thalamic input while CC neurons could sample from a larger subset of supragranular cells whose axons descend vertically into infragranular laminae (Jensen and Killackey 1987; Larsen and Callaway 2006). Such analyses of lamina-specific contributions of each cell type allow for neuronal morphology to be studied in the context of a larger cortical architecture.

Distinct electrical responses of excitatory L6 neuron subtypes

Physiological differences were observed between all three morphological types of pyramidal L6 neurons. Shorter mem-

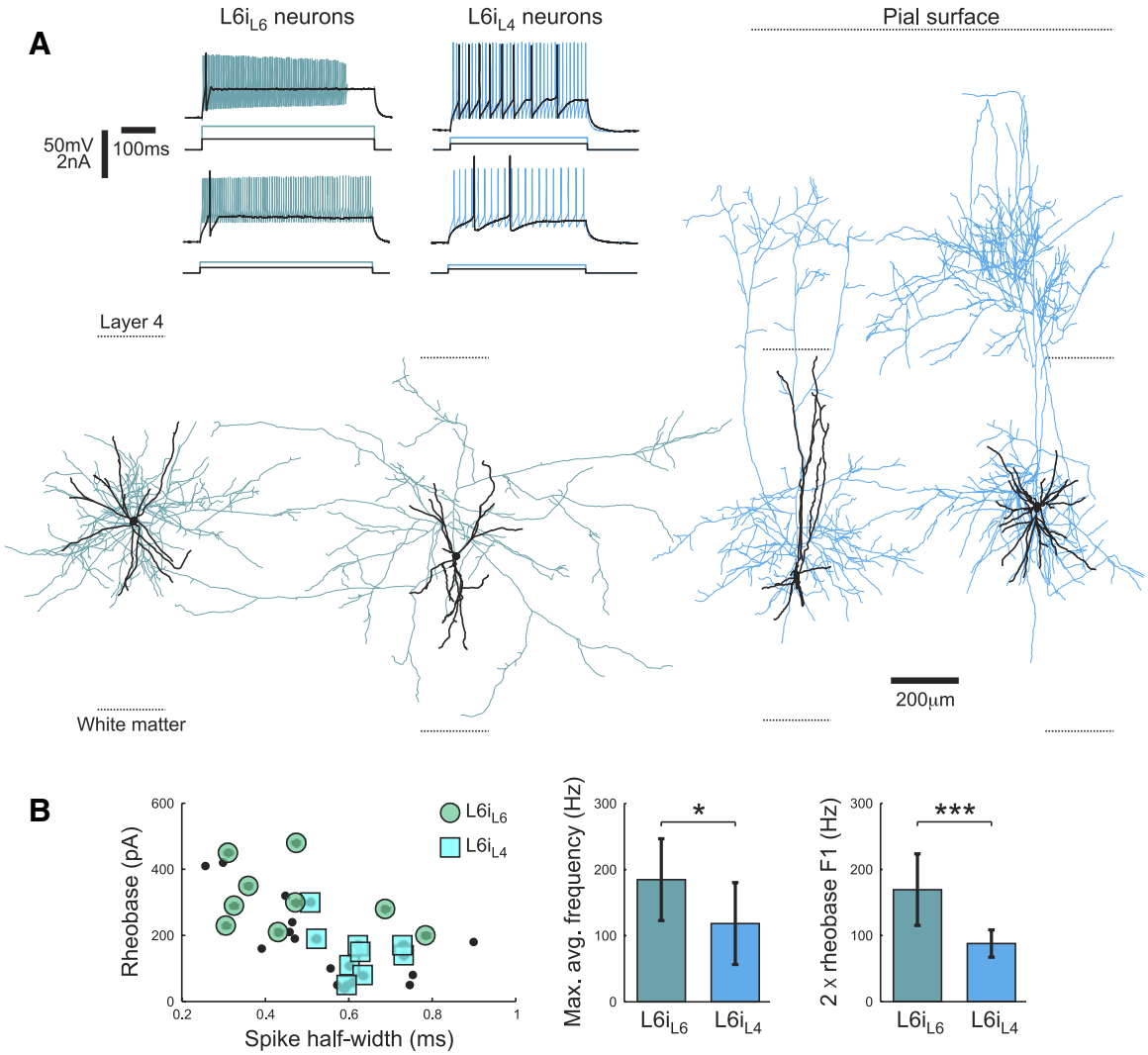

FIG. 5. Morphologically and physiologically distinct inhibitory cell types in L6. *A*: reconstructions of the dendrites and axons of 4 inhibitory neurons in L6 (dendrites and soma in black, axons in shades of blue; axonal reconstructions are incomplete). *Left*: the 2 neurons are examples of small and large basket cells, respectively (L6i$_{L6}$ neurons). *Right*: the axons of the 2 neurons are in contrast to the 1st 2 with branching both within L6 and also in granular and supragranular layers (L6i$_{L4}$ neurons). The spike trains in response to rheobase (black) and twice-rheobase (blue shades) currents for each neuron are shown above. *B, left*: the rheobase and spike half-widths of 32 L6i neurons recorded in this study (black dots). The neurons whose axonal morphology could be classified as L6i$_{L6}$ and L6i$_{L4}$ are indicated in circles and squares, respectively. *Right*: L6i$_{L6}$ neurons also fire spike trains of higher frequency than L6i$_{L4}$ (average frequencies in response to saturating currents and first instantaneous frequencies in response to twice-rheobase currents are plotted).

brane time constant and larger rheobase in CT neurons suggest shorter synaptic integration times compared with CC cells. Faster spike repolarization in CT neurons, presumably due to faster K^+ channels, results in narrower spikes, which would lead to smaller calcium currents, reduced transmitter release, and be reflected finally in the postsynaptic responses evoked by these neurons (Geiger and Jonas 2000; Ishikawa et al. 2003). Assuming similar differences in vivo, eliciting a spike in a CT cell would require stronger and more synchronous input than required to discharge CC neurons. CT cells may therefore respond selectively to strong principal-whisker stimulation, whereas CC neurons could reliably (owing to their burst-like responses) signal the presence of weak, nonspecific whisker deflections, e.g., air puffs. Evidence supporting such predictions come from reports that many L6 neurons in the rodent somatosensory cortex fail to respond to whisker stimulation and when they do, show a large variability in their latency (Armstrong-James et al. 1992; de Kock et al. 2007; Wilent and Contreras 2004). The extremely short latencies to surround whisker stimulation reported for neurons in this lamina (Carvell and Simons 1988) correspond with the wider dendritic fields, low rheobase, and burst-like responses of CC neurons.

While cells were encountered in both barrel and septal columns, it was often not possible to reliably assign cells to either category. The symmetrical dendritic morphology of each cell and homogeneity in the electrical properties of each excitatory cell population argue against the existence of distinct barrel and septal subpopulations. Differences in circuitry and functional responses with respect to barrels and septa remain to be tested.

Classification of excitatory L6 neurons

There are no known cytochemical markers that distinguish CT and CC neurons. While differences between L6 neurons

TABLE 3. *Physiological parameters of L6i$_{L6}$ and L6i$_{L4}$ interneurons*

Physiological Parameters	L6i$_{L6}$ (9)	L6i$_{L4}$ (9)	*P* Value	ROC Area	L6i (32)	L6e (72)	*P* Value	ROC Area
RMP, mV	−68.5 +/− 4.5	−67.9 +/− 7.0	0.86		−68.5 +/− 4.6	−70.4 +/− 4.1	4.3E-02	0.61
Input resistance, MΩ	97.7 +/− 43.5	132.6 +/− 37.3	0.12		128.2 +/− 48.8	149.3 +/− 51.8	0.12	
Membrane tau, ms	7.2 +/− 1.9	10.7 +/− 3.9	0.06		**9.6 +/− 3.5**	**14.4 +/− 4.1**	**1.2E-07**	**0.83**
Rheobase, pA	310.0 +/− 122.1	146.2 +/− 75.4	7.3E-03	0.89	205.2 +/− 124.7	162.8 +/− 74.8	0.15	
AP1 amplitude, mV	74.1 +/− 5.5	82.6 +/− 6.8	2.0E-02	0.88	**80.9 +/− 9.3**	**101.8 +/− 7.8**	**1.1E-20**	**0.96**
AP1 latency, ms	17.3 +/− 7.8	76.6 +/− 44.9	4.4E-03	0.96	**73.1 +/− 77.5**	**104.4 +/− 52.6**	**1.5E-05**	**0.72**
AP1 half-width, ms	**0.37 +/− 0.06**	**0.63 +/− 0.07**	**6.2E-06**	**1.00**	**0.54 +/− 0.16**	**0.90 +/− 0.19**	**5.3E-15**	**0.93**
AP1 rise slope, mV/ms	67.4 +/− 18.9	78.3 +/− 13.5	0.22		**76.9 +/− 21.9**	**102.4 +/− 20.8**	**1.9E-07**	**0.81**
AP1 fall slope, mV/ms	−117.8 +/− 24.8	−79.9 +/− 17.2	4.1E-03	0.93	**−94.5 +/− 27.2**	**−64.1 +/− 19.6**	**4.9E-09**	**0.82**
AP1 threshold-absolute, mV	−35.3 +/− 6.2	−37.6 +/− 6.2	0.49		**−36.4 +/− 5.5**	**−31.3 +/− 4.9**	**1.1E-05**	**0.76**
AP1 threshold-relative, mV	31.0 +/− 3.4	30.5 +/− 4.1	0.80		**32.0 +/− 4.9**	**39.1 +/− 4.5**	**1.3E-10**	**0.87**
AP1 fAHP amplitude, mV	−22.5 +/− 4.9	−17.2 +/− 4.8	0.06		**−19.7 +/− 4.3**	**−11.4 +/− 4.4**	**2.6E-14**	**0.91**
AP1 sAHP amplitude, mV						**−16.3 +/− 3.9**		
AP1 fAHP latency, ms	1.76 +/− 0.38	3.21 +/− 1.02	3.6E-03	0.96	**3.0 +/− 2.0**	**6.8 +/− 5.0**	**2.2E-07**	**0.82**
AP1 sAHP latency, ms						**41.9 +/− 30.4**		
Max avg frequency, Hz	**220.7 +/− 37.2**	**129.1 +/− 56.6**	**3.0E-03**	**0.96**	**146.7 +/− 76.6**	**44.4 +/− 14.5**	**2.6E-11**	**0.88**
Max 1st inst. frequency, Hz	258.3 +/− 37.7	184.0 +/− 61.3	1.6E-02	0.84	221.8 +/− 65.4	187.0 +/− 71.1	1.1E-02	0.65
Max 2nd inst. frequency, Hz	249.8 +/− 39.1	175.0 +/− 55.4	1.3E-02	0.89	**205.4 +/− 61.0**	**99.9 +/− 54.9**	**6.2E-10**	**0.88**
2×Rheobase: avg. freq., Hz	**165.0 +/− 49.9**	**63.8 +/− 32.5**	**7.3E-04**	**0.96**	**86.2 +/− 71.1**	**26.5 +/− 6.4**	**4.1E-08**	**0.74**
2×Rheobase: 1st inst. freq., Hz	**200.8 +/− 47.6**	**88.3 +/− 22.6**	**1.1E-04**	**1.00**	127.9 +/− 65.1	106.3 +/− 67.1	3.8E-02	0.62
2×Rheobase: 2nd inst. freq., Hz	**191.0 +/− 52.7**	**83.0 +/− 30.2**	**5.1E-04**	**0.96**	**116.1 +/− 66.5**	**46.3 +/− 30.2**	**8.0E-10**	**0.87**
2×Rheobase: adaptation index	24.6 +/− 14.1	29.1 +/− 23.9	0.67		**33.2 +/− 23.5**	**68.8 +/− 16.7**	**4.2E-12**	**0.88**
2×Rheobase: adaptation tau, ms	276.8 +/− 354.4	73.6 +/− 52.5	0.16		**153.1 +/− 257.3**	**12.9 +/− 12.1**	**7.8E-08**	**0.90**
IFavg fit: saturation freq, Hz	616.2 +/− 755.1	457.8 +/− 425.7	0.69		**477.0 +/− 608.7**	**70.7 +/− 32.9**	**5.6E-12**	**0.97**
IFavg fit: 1/slope	985.2 +/− 1764.9	1002.6 +/− 1132.7	0.81		960.5 +/− 1589.6	277.2 +/− 248.1	2.7E-02	0.65
IFavg fit: rheobase, pA	327.8 +/− 148.6	181.3 +/− 50.8	1.3E-02	0.89	241.8 +/− 133.6	176.4 +/− 74.9	5.0E-02	0.65
IFinst fit: saturation freq, Hz	397.0 +/− 132.7	812.3 +/− 980.2	0.29		**508.6 +/− 535.1**	**476.9 +/− 644.9**	**5.9E-04**	**0.64**
IFinst fit: 1/slope	301.3 +/− 222.6	1703.3 +/− 2401.8	0.06		813.1 +/− 1370.0	892.5 +/− 1668.8	0.06	
IFinst fit: rheobase, pA	**333.8 +/− 138.7**	**163.7 +/− 45.2**	**2.7E-04**	**1.00**	219.0 +/− 126.5	188.9 +/− 105.1	0.11	
IFinst fit slope/IFavg fit slope	1.15 +/− 0.81	1.49 +/− 0.85	0.44		1.35 +/− 0.97	4.38 +/− 6.72	1.4E-02	0.55

A comparison of physiological properties of L6i$_{L6}$ and L6i$_{L4}$ neurons (left) and of all excitatory and inhibitory L6 neurons (right). *P* values of *t*-tests and ROC areas for each differing parameter ($P < 0.05$) are listed. Parameters differing significantly after the Bonferroni correction ($P < 0.0031$) are indicated in bold.

have been reported based on the use of aspartate or glutamate as neurotransmitter (Kaneko et al. 1995), these have not been mapped onto the CT and CC populations (Conti et al. 1987; Giuffrida and Rustioni 1988). This study further stresses the stereotypical morphology of CT neurons; their thick descending axons, upward going collaterals, and dendritic tufts situated around L4 are unique features among infragranular neurons. CC cells, however, have varied dendritic morphologies (possibly representing different functional groups) and have in common the infragranular arborization of axon collaterals and an absence of a subcortical target. Furthermore, the morphological groups of L6e neurons can be reliably distinguished based on physiological features. Each parameter that differs significantly different between CT and CC neurons distinguishes them with 77–95% reliability (ROC areas in Table 2); combinations can result in a classification performance approaching 100% (Supplemental Fig. S1[1]).

While both CT and CC neurons in this study fired regular spike trains, sharp electrode recordings from CC-like neurons pooled across rat visual and somatosensory areas showed an exclusively phasic firing pattern (Mercer et al. 2005; West et al. 2006). In the mouse visual cortex, however, both cell types fired regular spike trains, but CT neurons were more excitable (Brumberg et al. 2003). CT neurons in this study had a higher rheobase; a similar current injection would result in slightly (but insignificantly) greater number of spikes in CC neurons (Fig. 4*C*). These inconsistencies could arise from ambiguity in neuronal identity (antidromic excitation or phasic firing not reliably identifying CC neurons) but may also reflect modality-specific (visual vs. somatosensory) differences because these cortices express distinct sets of genes and proteins tightly related to neural morphogenesis and connectivity (Leamey et al. 2008).

Inhibitory cell types in L6

Judging from their morphology, the inhibitory neurons in our study were a heterogeneous group. Nevertheless, two distinct interneuron types could be identified based on contrasting laminar innervation profiles, a scheme very similar to L6 of the macaque V1 (Lund et al. 1988), where the targeting of L4 by specific L6i subtypes is striking. The proportion of L6 interneurons with interlaminar projections is unknown, but it is unlikely to be small: 50% of recovered L6i neurons in this study were determined to have an upward projecting axon with branching in L4, similar to the estimated proportion of Martinotti cells in this layer (Markram et al. 2004; Wang et al. 2004).

L6i$_{L4}$ cells include a subset of somatostatin-expressing neurons (Ma et al. 2006) and could belong to the morphological class of either basket or Martinotti cells, both known to have ascending projections from infragranular laminae (Kisvárday et al. 1987; Wang et al. 2004). Similarly, L6i$_{L6}$ neurons could either be parvalbumin (PV)- or cholecystokinin (CCK)-expressing interneurons (Kawaguchi and Kondo 2002), each having characteristic physiological properties. While it is likely

[1] The online version of this article contains supplemental data.

that the two L6i subtypes defined here consist of more than one molecular and/or electrophysiological class (evidenced in the variation in Fig. 5*B*), their different axonal laminar profiles may be associated with contrasting synaptic properties (Cossart et al. 2006; Dumitriu et al. 2007; Kapfer et al. 2007), together contributing to distinct laminar interactions.

Functional implication of cortical subcircuits

This study emphasizes the functional links between layers 6 and 4. Both excitatory and inhibitory neurons selectively project from L6 to L4, thus linking the two major thalamorecepient laminae (Herkenham 1980; LeVay and Gilbert 1976). While the excitatory projection from L6 has been studied with its role in generating L4 receptive fields in mind (Ahmed et al. 1994; McGuire et al. 1984; Staiger et al. 1996; Stratford et al. 1996), inhibitory effects have also been observed in L4 following L6 stimulation (Hirsch 1995; Wirth and Lüscher 2004). $L6i_{L4}$ neurons, owing to their low rheobase, are likely to be the first cells responding to stimulation of L6 and could mediate the observed inhibition in L4. While the excitatory projection to L4, a branch of the corticothalamic projection, could be involved in synchronizing activity in thalamic neurons and thalamorecepient cortical neurons (Jones 2002), the role of the parallel inhibitory projection is less clear.

In summary, the morphologically and physiologically defined cell types in L6 likely constitute functionally distinct subcircuits. CT and $L6i_{L4}$ neurons link the two thalamorecepient laminae; CC and $L6i_{L6}$ cells mediate cross-columnar interactions in the infragranular laminae. Based on their physiological properties, CC and $L6i_{L4}$ cells are likely to respond to low-intensity stimuli, thus exciting infragranular activity across columns to nonspecific whisker stimuli, while inhibiting L4 neurons within the same column; stronger and more specific stimuli will evoke CT cell responses and recruit the high-rheobase, fast-spiking $L6i_{L6}$ cells. Such an interconnected network of neurons belonging to different subcircuits is likely to be a ubiquitous feature of cortex (Le Be et al. 2007; Morishima and Kawaguchi 2006); elaborating the structural and physiological properties of such networks is central to understanding cortical function.

ACKNOWLEDGMENTS

We thank S. Fusi for discussions, J. Hipp and T. Ott for help with statistical methods, S. Rickauer for reconstructions, D. Kuhl for support and discussions, L. Rettig for helpful comments. We are indebted to K. Martin for invaluable discussions, support, and reading previous versions of this manuscript.

GRANTS

This work was supported by an European Union Grant EU-FP6-2005 IST-1583 to K.A.C. Martin.

REFERENCES

Agmon A, Connors BW. Thalamocortical responses of mouse somatosensory (barrel) cortex in vitro. *Neuroscience* 41: 365–379, 1991.

Ahmed B, Anderson JC, Douglas RJ, Martin KA, Nelson JC. Polyneuronal innervation of spiny stellate neurons in cat visual cortex. *J Comp Neurol* 341: 39–49, 1994.

Ajima A, Tanaka S. Spatial patterns of excitation and inhibition evoked by lateral connectivity in layer 2/3 of rat barrel cortex. *Cereb Cortex* 16: 1202–1211, 2006.

Armstrong-James M, Fox K, Das-Gupta A. Flow of excitation within rat barrel cortex on striking a single vibrissa. *J Neurophysiol* 68: 1345–1358, 1992.

Bekkers JM, Häusser M. Targeted dendrotomy reveals active and passive contributions of the dendritic tree to synaptic integration and neuronal output. *Proc Natl Acad Sci USA* 104: 11447–11452, 2007.

Brumberg JC, Hamzei-Sichani F, Yuste R. Morphological and physiological characterization of layer VI corticofugal neurons of mouse primary visual cortex. *J Neurophysiol* 89: 2854–2867, 2003.

Carvell GE, Simons DJ. Membrane potential changes in rat SmI cortical neurons evoked by controlled stimulation of mystacial vibrissae. *Brain Res* 448: 186–191, 1988.

Conti F, Rustioni A, Petrusz P. Co-localization of glutamate and aspartate immunoreactivity in neurons of the rat somatic sensory cortex. In: *Excitatory Amino Acid Transmission,* edited by Hicks TP, Lodge D, McLennan H. New York: Liss, 1987, p. 160–172.

Cossart R, Petanjek Z, Dumitriu D, Hirsch JC, Ben-Ari Y, Esclapez M, Bernard C. Interneurons targeting similar layers receive synaptic inputs with similar kinetics. *Hippocampus* 16: 408–420, 2006.

de Kock CPJ, Bruno RM, Spors H, Sakmann B. Layer- and cell-type-specific suprathreshold stimulus representation in rat primary somatosensory cortex. *J Physiol* 581: 139–154, 2007.

Dumitriu D, Cossart R, Huang J, Yuste R. Correlation between axonal morphologies and synaptic input kinetics of interneurons from mouse visual cortex. *Cereb Cortex* 17: 81–91, 2007.

Ferrer I, Fabregues I, Condom E. A Golgi study of the sixth layer of the cerebral cortex. I. The lissencephalic brain of *Rodentia, Lagomorpha, Insectivora* and *Chiroptera. J Anat* 145: 217–234, 1986.

Fitzpatrick D, Lund JS, Blasdel GG. Intrinsic connections of macaque striate cortex: afferent and efferent connections of lamina 4C. *J Neurosci* 5: 3329–3349, 1985.

Geiger JR, Jonas P. Dynamic control of presynaptic Ca(2+) inflow by fast-inactivating K(+) channels in hippocampal mossy fiber boutons. *Neuron* 28: 927–939, 2000.

Gilbert CD, Kelly JP. The projections of cells in different layers of the cat's visual cortex. *J Comp Neurol* 163: 81–105, 1975.

Gilbert CD, Wiesel TN. Morphology and intracortical projections of functionally characterised neurons in the cat visual cortex. *Nature* 280: 120–125, 1979.

Giuffrida R, Rustioni A. Glutamate and aspartate immunoreactivity in corticothalamic neurons in rats. In: *Cellular Thalamic Mechanisms,* edited by Bentivoglio M, Spreafico R. Amsterdam: Elsevier, 1988, p. 311–320.

Gupta A, Wang Y, Markram H. Organizing principles for a diversity of GABAergic interneurons and synapses in the neocortex. *Science* 287: 273–278, 2000.

Herkenham M. Laminar organization of thalamic projections to the rat neocortex. *Science* 207: 532–535, 1980.

Hirsch JA. Synaptic integration in layer IV of the ferret striate cortex. *J Physiol* 483: 183–199, 1995.

Hutsler JJ, Lee DG, Porter KK. Comparative analysis of cortical layering and supragranular layer enlargement in rodent carnivore and primate species. *Brain Res* 1052: 71–81, 2005.

Ishikawa T, Nakamura Y, Saitoh N, Li WB, Iwasaki S, Takahashi T. Distinct roles of Kv1 and Kv3 potassium channels at the calyx of Held presynaptic terminal. *J Neurosci* 23: 10445–10453, 2003.

Jensen KF, Killackey HP. Terminal arbors of axons projecting to the somatosensory cortex of the adult rat. I. The normal morphology of specific thalamocortical afferents. *J Neurosci* 7: 3529–3543, 1987.

Jones EG. Thalamic circuitry and thalamocortical synchrony. *Philos Trans R Soc Lond B Biol Sci* 357: 1659–1673, 2002.

Kampa BM, Letzkus JJ, Stuart GJ. Cortical feed-forward networks for binding different streams of sensory information. *Nat Neurosci* 9: 1472–1473, 2006.

Kaneko T, Kang Y, Mizuno N. Glutaminase-positive and glutaminase-negative pyramidal cells in layer VI of the primary motor and somatosensory cortices: a combined analysis by intracellular staining and immunocytochemistry in the rat. *J Neurosci* 15: 8362–8377, 1995.

Kaneko T, Saeki K, Lee T, Mizuno N. Improved retrograde axonal transport and subsequent visualization of tetramethylrhodamine (TMR)-dextran amine by means of an acidic injection vehicle and antibodies against TMR. *J Neurosci Methods* 65: 157–165, 1996.

Kapfer C, Glickfeld LL, Atallah BV, Scanziani M. Supralinear increase of recurrent inhibition during sparse activity in the somatosensory cortex. *Nat Neurosci* 10: 743–753, 2007.

Katz LC. Local circuitry of identified projection neurons in cat visual cortex brain slices. *J Neurosci* 7: 1223–1249, 1987.

Kawaguchi Y, Kondo S. Parvalbumin, somatostatin and cholecystokinin as chemical markers for specific GABAergic interneuron types in the rat frontal cortex. *J Neurocytol* 31: 277–287, 2002.

Killackey HP, Sherman SM. Corticothalamic projections from the rat primary somatosensory cortex. *J Neurosci* 23: 7381–7384, 2003.

Kisvárday ZF, Martin KA, Friedlander MJ, Somogyi P. Evidence for interlaminar inhibitory circuits in the striate cortex of the cat. *J Comp Neurol* 260: 1–19, 1987.

Koralek KA, Jensen KF, Killackey HP. Evidence for two complementary patterns of thalamic input to the rat somatosensory cortex. *Brain Res* 463: 346–351, 1988.

Land PW, Kandler K. Somatotopic organization of rat thalamocortical slices. *J Neurosci Methods* 119: 15–21, 2002.

Land PW, Simons DJ. Cytochrome oxidase staining in the rat smI barrel cortex. *J Comp Neurol* 238: 225–235, 1985.

Larsen DD, Callaway EM. Development of layer-specific axonal arborizations in mouse primary somatosensory cortex. *J Comp Neurol* 494: 398–414, 2006.

Le Be JV, Silberberg G, Wang Y, Markram H. Morphological, electrophysiological, and synaptic properties of corticocallosal pyramidal cells in the neonatal rat neocortex. *Cereb Cortex* 17: 2204–2213, 2007.

Leamey CA, Glendining KA, Kreiman G, Kang ND, Wang KH, Fassler R, Sawatari A, Tonegawa S, Sur M. Differential gene expression between sensory neocortical areas: potential roles for Ten_m3 and Bcl6 in patterning visual and somatosensory pathways. *Cereb Cortex* 18: 53–66, 2008.

LeVay S, Gilbert CD. Laminar patterns of geniculocortical projection in the cat. *Brain Res* 113: 1–19, 1976.

Lund JS. Anatomical organization of macaque monkey striate visual cortex. *Annu Rev Neurosci* 11: 253–288, 1988.

Lund JS, Hawken MJ, Parker AJ. Local circuit neurons of macaque monkey striate cortex. II. Neurons of laminae 5B and 6. *J Comp Neurol* 276: 1–29, 1988.

Ma Y, Hu H, Berrebi AS, Mathers PH, Agmon A. Distinct subtypes of somatostatin-containing neocortical interneurons revealed in transgenic mice. *J Neurosci* 26: 5069–5082, 2006.

Mainen ZF, Sejnowski TJ. Influence of dendritic structure on firing pattern in model neocortical neurons. *Nature* 382: 363–366, 1996.

Markram H, Toledo-Rodriguez M, Wang Y, Gupta A, Silberberg G, Wu C. Interneurons of the neocortical inhibitory system. *Nat Rev Neurosci* 5: 793–807, 2004.

Martin KA, Somogyi P, Whitteridge D. Physiological and morphological properties of identified basket cells in the cat's visual cortex. *Exp Brain Res* 50: 193–200, 1983.

McGuire BA, Hornung JP, Gilbert CD, Wiesel TN. Patterns of synaptic input to layer 4 of cat striate cortex. *J Neurosci* 4: 3021–3033, 1984.

Mercer A, West DC, Morris OT, Kirchhecker S, Kerkhoff JE, Thomson AM. Excitatory connections made by presynaptic cortico-cortical pyramidal cells in layer 6 of the neocortex. *Cereb Cortex* 15: 1485–1496, 2005.

Morishima M, Kawaguchi Y. Recurrent connection patterns of corticostriatal pyramidal cells in frontal cortex. *J Neurosci* 26: 4394–4405, 2006.

Prieto JJ, Winer JA. Layer VI in cat primary auditory cortex: Golgi study and sublaminar origins of projection neurons. *J Comp Neurol* 404: 332–358, 1999.

Rauch A, La Camera G, Luscher HR, Senn W, Fusi S. Neocortical pyramidal cells respond as integrate-and-fire neurons to in-vivo-like input currents. *J Neurophysiol* 90: 1598–1612, 2003.

Ren JQ, Aika Y, Heizmann CW, Kosaka T. Quantitative analysis of neurons and glial cells in the rat somatosensory cortex with special reference to GABAergic neurons and parvalbumin-containing neurons. *Exp Brain Res* 92: 1–14, 1992.

Ribak CE. Aspinous and sparsely-spinous stellate neurons in the visual cortex of rats contain glutamic acid decarboxylase. *J Neurocytol* 7: 461–478, 1978.

Rouiller EM, Welker E. A comparative analysis of the morphology of corticothalamic projections in mammals. *Brain Res Bull* 53: 727–741, 2000.

Skoglund TS, Pascher R, Berthold CH. Heterogeneity in the columnar number of neurons in different neocortical areas in the rat. *Neurosci Lett* 208: 97–100, 1996.

Staiger JF, Zilles K, Freund TF. Recurrent axon collaterals of corticothalamic projection neurons in rat primary somatosensory cortex contribute to excitatory and inhibitory feedback-loops. *Anat Embryol* 194: 533–543, 1996.

Stratford KJ, Tarczy-Hornoch K, Martin KA, Bannister NJ, Jack JJ. Excitatory synaptic inputs to spiny stellate cells in cat visual cortex. *Nature* 382: 258–261, 1996.

Tömböl T. Layer VI cells. In: *Cerebral Cortex,* edited by Peters A, Jones EG. New York: Plenum, 1984, p. 479–519.

Usrey WM, Fitzpatrick D. Specificity in the axonal connections of layer VI neurons in tree shrew striate cortex: evidence for distinct granular and supragranular systems. *J Neurosci* 16: 1203–1218, 1996.

van Brederode JF, Snyder GL. A comparison of the electrophysiological properties of morphologically identified cells in layers 5B and 6 of the rat neocortex. *Neuroscience* 50: 315–337, 1992.

Wang Y, Gupta A, Toledo-Rodriguez M, Wu CZ, Markram H. Anatomical, physiological, molecular and circuit properties of nest basket cells in the developing somatosensory cortex. *Cereb Cortex* 12: 395–410, 2002.

Wang Y, Toledo-Rodriguez M, Gupta A, Wu C, Silberberg G, Luo J, Markram H. Anatomical, physiological and molecular properties of Martinotti cells in the somatosensory cortex of the juvenile rat. *J Physiol* 561: 65–90, 2004.

West DC, Mercer A, Kirchhecker S, Morris OT, Thomson AM. Layer 6 cortico-thalamic pyramidal cells preferentially innervate interneurons and generate facilitating EPSPs. *Cereb Cortex* 16: 200–211, 2006.

Wilent WB, Contreras D. Synaptic responses to whisker deflections in rat barrel cortex as a function of cortical layer and stimulus intensity. *J Neurosci* 24: 3985–3998, 2004.

Wirth C, Lüscher HR. Spatiotemporal evolution of excitation and inhibition in the rat barrel cortex investigated with multielectrode arrays. *J Neurophysiol* 91: 1635–1647, 2004.

Wise SP, Jones EG. Cells of origin and terminal distribution of descending projections of the rat somatic sensory cortex. *J Comp Neurol* 175: 129–157, 1977.

Wong-Riley MT, Welt C. Histochemical changes in cytochrome oxidase of cortical barrels after vibrissal removal in neonatal and adult mice. *Proc Natl Acad Sci USA* 77: 2333–2337, 1980.

Yoshimura Y, Dantzker JL, Callaway EM. Excitatory cortical neurons form fine-scale functional networks. *Nature* 433: 868–873, 2005.

Zarrinpar A, Callaway EM. Local connections to specific types of layer 6 neurons in the rat visual cortex. *J Neurophysiol* 95: 1751–1761, 2006.

Zhang ZW, Deschênes M. Intracortical axonal projections of lamina VI cells of the primary somatosensory cortex in the rat: a single-cell labeling study. *J Neurosci* 17: 6365–6379, 1997.